



# Tunable periodic graphene antidot lattices fabricated by e-beam lithography and oxygen ion etching



L.Z. Liu<sup>a,b</sup>, S.B. Tian<sup>a</sup>, Y.Z. Long<sup>b</sup>, W.X. Li<sup>a</sup>, H.F. Yang<sup>a</sup>, J.J. Li<sup>a,\*</sup>, C.Z. Gu<sup>a,\*</sup>

<sup>a</sup> Beijing National Laboratory for Condensed Matter Physics, Institute of Physics, Chinese Academy of Sciences, Beijing 100190, China

<sup>b</sup> College of Physics Science, Qingdao University, Qingdao 266071, China

## ARTICLE INFO

### Article history:

Received 31 October 2013

Received in revised form

10 January 2014

Accepted 11 January 2014

### Keywords:

Patterning graphene

Antidot lattices

EBL

RIE

## ABSTRACT

Intrinsic monolayer graphene has no band gap between its conduction and valence bands, which limits its application in many aspects as a semiconductor. Antidot lattices by constructing periodic holes on graphene have been proved to be an intriguing strategy to introduce a band gap into graphene. Here we used the e-beam lithography (EBL) combined with the oxygen reactive ion etching (RIE) to fabricate tunable antidot lattices with different and uniform regularly spaced holes on graphene. In this way, tunable periodic graphene nanostructures with the dimensions ranging from  $\sim 20$  nm to several hundreds of nanometers can be fabricated by controlling exposure dose and etching time.

© 2014 Elsevier Ltd. All rights reserved.

## 1. Introduction

Since its experimental discovery in 2004 [1], graphene has attracted extraordinary attention owing to its many outstanding physical properties, such as high mobility [2], quantum electronic transport [3], room-temperature quantum Hall effect [4], high elasticity [5] and good optical transparency [6]. Many potential electronic applications of graphene have also been demonstrated or proposed as transparent conductors [7], spintronic devices [8], sensors [9,10] and flexible electronics devices [11,12], but the deficiency of band gap around the Fermi level limits graphene application as a semiconductor material. However, graphene can show tunable band gap characteristics by adjusting size, shape, or surface functionalization [13]. Several kinds of structures have been proposed to introduce a band gap into graphene, such as nanoribbon, nanomesh and quantum dots [14–16]. Among these structures, graphene nanoribbon devices are the most commonly used, but they have relatively low driving currents or conductance for graphene-based semiconductor devices [17]. Therefore, in order to improve the performances of the graphene-based devices, the dense arrays of ordered nanoribbons will be required, which is still a great challenge.

Recently, a strategy of constructing periodic holes on graphene to form graphene antidot lattices has been extensively proposed. Graphene antidot lattices consist of the holes of a periodic arrangement in a graphene sheet [18]. Theoretical calculations have predicted that antidot lattices can introduce a band gap in graphene, and the width of opened gap can be tuned by the size, shape, and symmetry of both the hole and the lattice cell [19,20]. Some experimental studies have demonstrated that graphene antidot lattice have an effective energy gap of 100 meV and field effect transistors have an ON – OFF current ratio of up to 10, which demonstrate the utility of these structures for applications [21,22]. In comparison with a single nanoribbon, graphene antidot lattices can ensure a higher drive current when used as a conduction channel. More importantly, it is also an important foundation for constructing graphene superlattices with various nanoscopic functional units. To widening their application range in electronic devices, various methods such as lithography, nanoimprinting, and chemical techniques have been used to fabricate patterning graphene. Comparing other approaches of preparation of graphene antidot lattices, EBL combined with RIE as the most commonly used method have a lot of advantages, such as accurate alignment accuracy, high pattern resolution, large scale area, good uniformity and arbitrary control the size of antidot lattice. However, how to fabricate large-scale, uniform and high-density antidot lattice by using EBL and RIE is still a great challenge due to the well-known electron scattering effects in common electron beam photoresists and the uncertainty during reactive ions etching. In this work, we carried out EBL and RIE technique to fabricate tunable antidot

\* Corresponding authors. Tel.: +86 10 82649097; fax: +86 10 82648198.

E-mail addresses: [jjli@aphy.iphy.ac.cn](mailto:jjli@aphy.iphy.ac.cn) (J.J. Li), [czgu@aphy.iphy.ac.cn](mailto:czgu@aphy.iphy.ac.cn) (C.Z. Gu).

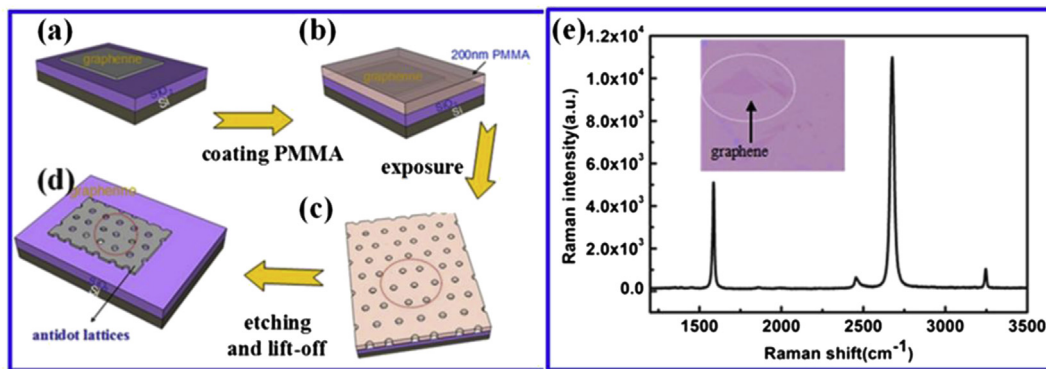


**Fig. 1.** A schematic illustration of the simple and scalable graphene patterning processes. (a) Natural graphene deposited on SiO<sub>2</sub> (300 nm)/Si substrate. (b) A layer of PMMA was coated on the top of graphene. (c) EBL was used to pattern the PMMA into desired shapes at desired locations. (d) RIE was used to etch graphene/PMMA film. (e) Raman spectrum of monolayer graphene on SiO<sub>2</sub>/Si substrate and the inset shows the optical microscope photograph of the graphene.

lattices, and different and uniform regularly spaced holes on graphene were achieved by controlling exposure dose and etching time. Finally, large-scale, uniform and dense grid of antidot lattices on graphene were fabricated successfully. Our results indicate that accurate control in both exposure dose and etching time is very desired approach to fabricate tunable antidot lattices nanostructures on graphene.

## 2. Experiment

**Fig. 1** shows the schematic illustration of our fabricating procedure. Initially, the monolayer graphene was deposited on SiO<sub>2</sub>(300 nm)/Si substrate by mechanical exfoliation [Fig. 1(a)]. Then a layer of PMMA (about 200 nm) was coated on the top of graphene [Fig. 1(b)]. By changing exposure dose of EBL system (Raith 150), antidot lattices with different periods were formed on the PMMA layer [Fig. 1(c)]. After exposure, the sample was developed in methyl isobutyl ketone: isopropyl alcohol (IPA) (1:3) for 40 s and IPA for 30 s, and then was dried using pure nitrogen. Finally, short time (around 10–16 s) based on oxygen etching (O<sub>2</sub> flow: 100 sccm; Pressure: 100 mTorr; Power: 100 W) didn't influence the overall quality of antidot lattices on graphene flake. After lift-off was done in hot acetone ( $T = 80\text{ }^{\circ}\text{C}$ ) about 5 min in order to remove photoresist on the graphene [Fig. 1(d)].

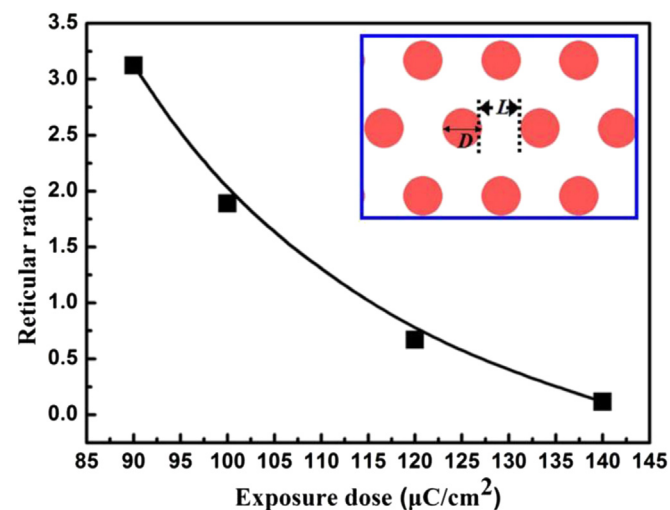


**Fig. 2.** The change tendency of reticular ratio with different exposure dose, and the reticular ratio ( $L/D$ ) represents the ratio of hole space ( $L$ ) to hole diameter ( $D$ ).

## 3. Results and discussion

**Fig. 1(e)** shows a typical Raman spectrum of graphene on SiO<sub>2</sub>/Si substrate. There are two prominent peaks (G and 2D) and two small peaks (G' and 2D'). Two intense peaks are the G band at  $1585\text{ cm}^{-1}$ , and the 2D band at  $2676\text{ cm}^{-1}$ , respectively. The G peak corresponds to the stretching vibration mode, E<sub>2g</sub> phonon at the Brillouin zone center. The 2D peak originates from a two phonon double resonance Raman process, and it is always present for crystalline carbon materials [23]. The intensity of 2D peak is more than twice that those of G peak and the full width at half maximum (FWHM) of 2D band is  $29\text{ cm}^{-1}$ , suggesting that the sample is monolayer graphene. The Raman G' band ( $\sim 2450\text{ cm}^{-1}$ ) has a small intensity, which originates from a combination of the zone boundary inplane longitudinal acoustic phonon and the inplane transverse optical phonon modes [24]. The 2D' peak ( $\sim 3250\text{ cm}^{-1}$ ) can be assigned to the second harmonic of D peak ( $\sim 1620\text{ cm}^{-1}$ ) [25], which does not require the existence of defects for its activation and is always present in the Raman spectrum of high-quality monolayer graphene. Moreover, it is noted that the D band in the Raman spectrum is not obvious, indicating the good crystalline structure of the graphene sample with few defects and impurities. The inset of **Fig. 1(e)** shows the optical microscope photograph of

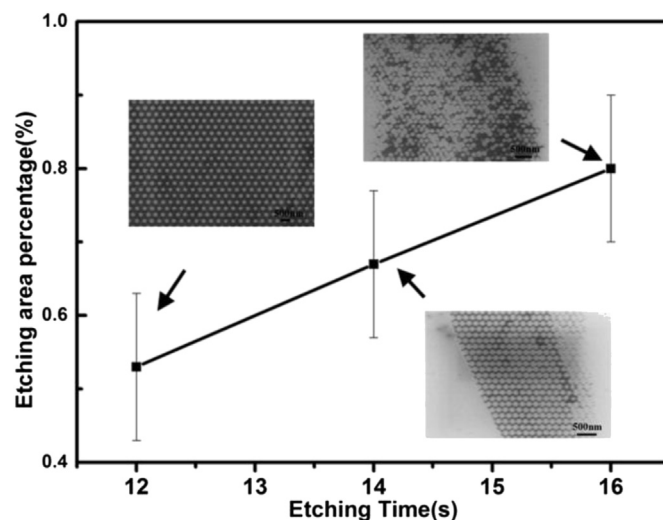


**Fig. 3.** The measured average etching area percentage of graphene antidot lattices change with the duration of plasma etching under a given O<sub>2</sub>-based RIE condition.

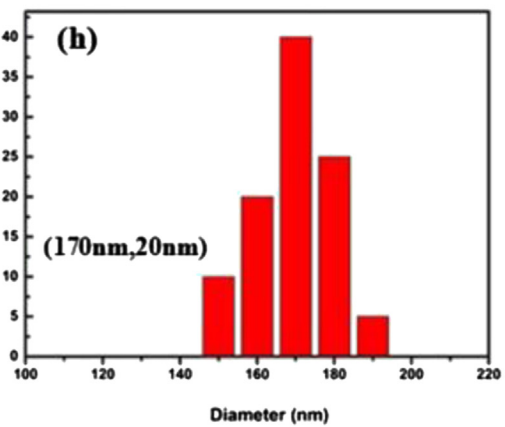
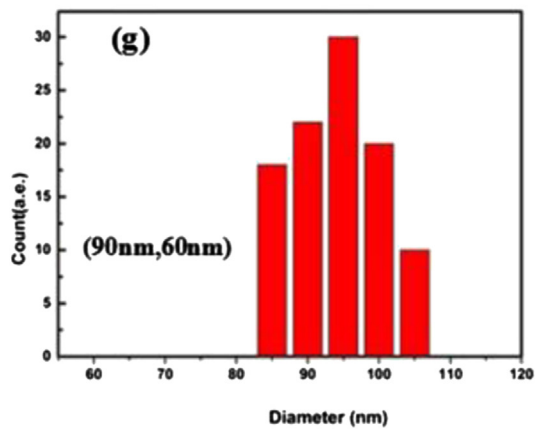
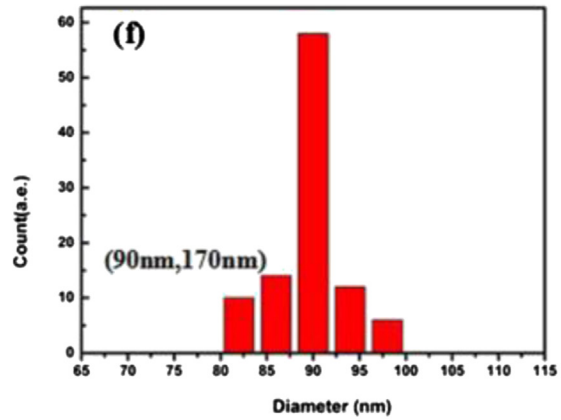
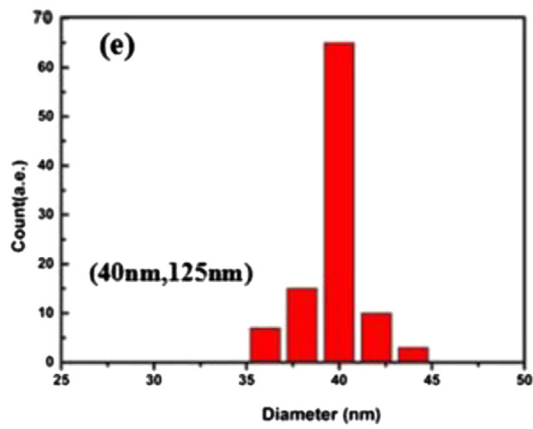
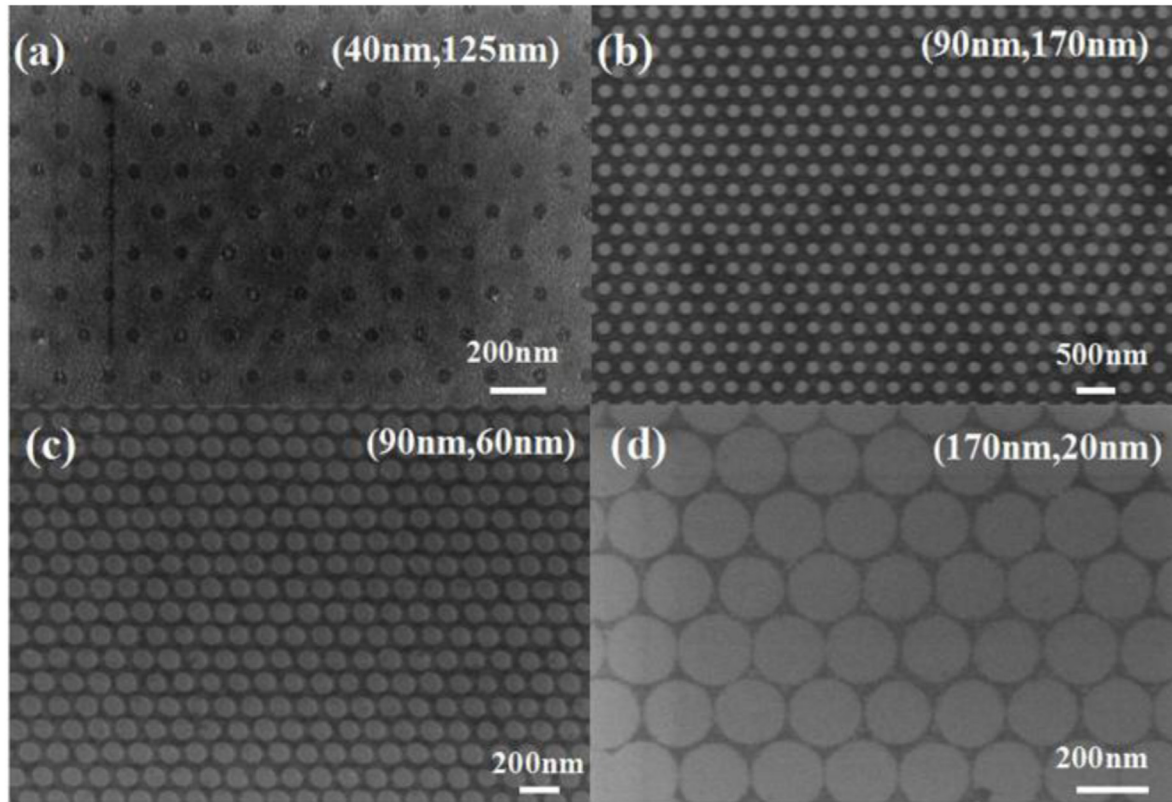


**Fig. 4.** (a–d) Different regularly spaced holes on graphene. The top right corner of the image shows the size of antidot lattices. ( $D, L$ ) represents hole diameter ( $D$ ) and hole space ( $L$ ); (e–h) the histogram of the diameter of antidot lattice with different period distributions.

the graphene, and it can be seen that the color of the sample is quite uniform, and it means that the entire sample is the monolayer graphene.

In the process of fabricating tunable antidot lattices, the exposure dose and etching time are the most important factors in the process of using EBL combined with RIE. It is well-known that all electron scattering effects existed in common electron beam photoresists. Thus, it is necessary to control periodicity and neck width by regulating exposure dose. In regard to the influence of the etching time, suitable etching time is conducive to the exposure graphics accurately transferred to the graphene. Only accurately controlled both the exposure dose and etching time at the same time, large-scale, uniform and dense grid of antidot lattices on graphene are obtained. Therefore, we attempt to find out the optimal parameters of preparing antidot lattices by optimizing exposure dose and etching time, respectively.

### 3.1. Exposure dose optimization

For the exposure process, the incident electrons lead to a small angle scattering after the interaction with PMMA. When the period space of antidot lattices is approximately equal to the scattering spread scope, the exposure dose will be a little larger than that of anticipation at each point. The radiation energy absorbed by each point in the PMMA is a sum of the direct radiation energy and surrounding scattered energy. Due to the proximity effect existing in photoresist exposure [26], actual exposure size of antidot lattices changes greatly compared with the designed graphic size.

Hence, different periodic antidot lattices are tuned by adjusting the area dose for different regularly spaced holes on graphene. Actually, it is found that there was a dependency between reticular ratio and different exposure dose. The reticular ratio ( $L/D$ ) represents the ratio of hole space ( $L$ ) to hole diameter ( $D$ ), as shown in the inset of Fig. 2. It can be seen that exposure dose needs to be changed with the hole diameter and space (from 90 to 140  $\mu\text{C}/\text{cm}^2$ ). As the exposure dose increases, the reticular ratio decreases accordingly. It results from the fact that the high reticular ratio is equivalent to low exposure density, or less scattered electron energy. So it is necessary to decrease the direct radiation energy to achieve the high reticular ratio.

### 3.2. Etching time optimization

RIE has many outstanding advantages, such as high etching rate, good anisotropy, large-area uniformity, high-quality fine etching line and profile. The patterned graphene was affected by many factors, such as etching time, gas flow rate, RF power and pressure. Among these factors, etching time is a quite key factor in the process of graphic transfer. By optimizing the time factor continuously, we found that short time (around 10–16 s) based on oxygen etching didn't influence the overall quality of antidot lattices on graphene flake. As we can see from Fig. 3, it is notable that etching monolayer graphene needs about 12 s in the  $\text{O}_2$  plasma etching process. If the etching time is more than 12 s, both the photoresist residual layer and the underlying graphene are etched away. In addition, over etching can result in a lateral etching of the hole diameter in the photoresist as well as the graphene, and thus increases the etching area percentage.

### 3.3. Fabrication results

It has been demonstrated above that antidot lattices with different periods can be obtained by optimizing etching conditions with exposure dose. Fig. 4(a–d) show different regularly spaced holes on graphene that were etched using PMMA (thickness of

200 nm) pattern as masks. The exposure dose is 90, 100, 120 and 140  $\mu\text{C}/\text{cm}^2$ , respectively. Meanwhile, the duration of plasma etching under the given  $\text{O}_2$ -based RIE condition is about 12 s. The space of antidot lattices range from 170 nm down to 20 nm. As we can see from Fig. 4(e–h), we can find that both the diameter and space of the holes present very good consistency and uniformity which is a promising candidate for opening band gap and has potential applications in integrated electronic and optoelectronic devices. In addition, an increased dispersion of hole diameter of graphene after etching can be observed with the decrease of the exposure dose from Fig. 4(e) to Fig. 4(h). This is because a lower radiation energy leads to an enhanced random scatter effect that can influence the distribution uniformity of radiation energy and hence a dispersion of hole diameter. But compared with some reported results, our fabricating graphene antidot lattices nanostructures have still obvious advantages in uniformity and tunable hole diameter size.

## 4. Conclusion

We have fabricated large-scale, uniform and different periods of antidot lattices on graphene by optimizing exposure dose of EBL and etching time of RIE, which demonstrated the convenience of tunable fabricating graphene patterns with high resolution and high alignment accuracy by EBL combined with RIE. Our experimental results provide a possible route of constructing graphene superlattices structures. It is also indicated that an optimized fabrication process can directly benefit the electronic applications of graphene as well.

## Acknowledgments

This work is supported by the NSFC (Grand No. 11174362, 91023041, 51272278, 61390503, 91323304), and the Knowledge Innovation Project of CAS (Grand No. KJCX2-EW-W02).

## References

- [1] Novoselov KS, Geim AK, Morozov SV, Jiang D, Zhang Y, Dubonos SV, et al. Electric field effect in atomically thin carbonfilms. *Science* 2004;306:666.
- [2] Geim AK, Novoselov KS, Morozov SV, Hill EW, Blake P, Katsnelson MI, et al. Detection of individual gas molecules adsorbed on graphene. *Nat Mater* 2007;6:183.
- [3] Abanin DA, Levitov LS, Marcus CM. Quantum Hall effect in a gate-controlled p-n junction of graphene. *Science* 2007;317:641–3.
- [4] Novoselov KS, Geim AK, Morozov SV, Jiang D, Katsnelson MI, Grigorieva IV, et al. Two-dimensional gas of massless Dirac fermions in graphene. *Nature* 2005;438:197.
- [5] Lee CG, Wei XD, Kysar JW, Hone J. Measurement of the elastic properties and intrinsic strength of monolayer graphene. *Science* 2008;321:385–8.
- [6] Zhu Y, Murali S, Cai W, Li X, Suk JW, Potts JR, et al. Graphene and graphene oxide: synthesis, properties, and applications. *Adv Mater* 2010;22:3906.
- [7] Watcharotone S, Dikin DA, Stankovich S, Piner I, Jung I, Domett GH, et al. Graphene-silica composite thin films as transparent conductors. *Nano Lett* 2007;7:7.
- [8] Candini A, Klyatskaya S, Ruben M, Wernsdorfer W, Affronte Marco. Graphene spintronic devices with molecular nanomagnets. *Nano Lett* 2011;11:2634–9.
- [9] Yoon HJ, Jun DH, Yang JH, Yang SS, Zhou Z, Cheng MM. Carbon dioxide gas sensor using a graphene sheet. *Sensors Actuators B* 2011;157:310–3.
- [10] Zhang ZG, Li Q, Li ZJ, Zhou QJ, Fang Y. Suspended graphene sensors with improved signal and reduced noise. *Nano Lett* 2010;10(5):1864–8.
- [11] Kim KS, Zhao Y, Jang H, Lee SY, Kim JM, Kim KS, et al. Large-scale pattern growth of graphene films for stretchable transparent electrodes. *Nature* 2009;457:5.
- [12] Wang D, Li F, Zhao J, Ren W, Chen ZG, Tan J, et al. Fabrication of graphene/polyaniline composite paper via in situ anodic electropolymerization for high-performance flexible electrode. *ACS Nano* 2009;3(7):1745–52.
- [13] Lee J, Kim K, Park WI, Kim B, Park JH, Kim T, et al. Uniform graphene quantum dots patterned from self-assembled silica nanodots. *Nano Lett* 2012;12:6078–83.
- [14] Li XL, Wang XR, Zhang L, Lee SW, Dai HJ. Chemically derived ultrasmooth graphene nanoribbon semiconductors. *Science* 2008;319:1229–32.

- [15] Han MY, Özyilmaz B, Zhang Y, Kim P. Energy band-gap engineering of graphene nanoribbons. *PRL* 2007;98:206805.
- [16] Bai JW, Zhong X, Jiang S, Huang Y, Duan XF. Graphene nanomesh. *Nat Nanotechnol* 2010;5:190–4.
- [17] Duan X. Assembled semiconductor nanowire thin films for high-performance flexible macroelectronics. *MRS Bull* 2007;32:134–41.
- [18] Pedersen TG, Flindt C, Pedersen J, Mortensen NA, Jauho AP, Pedersen K. Graphene antidot lattices: designed defects and spin qubits. *Phys Rev Lett* 2008;100:136804.
- [19] Furst JA, Pedersen JG, Flindt C, Mortensen NA, Brandbyge M, Pedersen TG, et al. Electronic properties of graphene antidot lattices. *New J Phys* 2009;11:095020.
- [20] Liu W, Wang ZF, Shi QW, Yang JL, Liu F. Band-gap scaling of graphene nanohole superlattices. *Phys Rev B* 2009;80:233405.
- [21] Liang XG, Jung YS, Wu S, Ismach A, Olynick DL, Cabrini S, et al. Formation of bandgap and subbands in graphene nanomeshes with sub-10 nm ribbon width fabricated via nanoimprint lithography. *Nano Lett* 2010;10:2454–60.
- [22] Kim M, Safron NS, Han E, Arnold MS, Gopalan P. Fabrication and characterization of large-area, semiconducting nanoperforated graphene materials. *Nano Lett* 2010;10:1125–31.
- [23] Mafra DL, Samsonidze G, Malard LM, Elias DC, Brant JC, Plentz F, et al. Determination of LA and TO phonon dispersion relations of graphene near the dirac point by double resonance Raman scattering. *Phys Rev B* 2007;76:233407.
- [24] Tan PH, Deng YM, Zhao Q. Temperature-dependent Raman spectra and anomalous Raman phenomenon of highly oriented pyrolytic graphite. *Phys Rev B* 1998;58:5435–9.
- [25] Li J, Chen JT, Shen BS, Yan XB, Qun QJ. Temperature dependence of the field emission from the few-layer graphene film. *Appl Phys Lett* 2011;99:163103.
- [26] Chang THP. Proximity effect in electron lithography. *J Vac Sci Technol* 1975;12:1271.